Article:

Barr, A. orcid.org/0000-0002-8240-6412, Rigby, S.E., Collins, R. et al. (2 more authors) (2020) Predicting crater formation from failure of pressurized water mains through analogy with buried explosive events. Journal of Pipeline Systems Engineering and Practice, 11 (2). 04020013. ISSN 1949-1190

https://doi.org/10.1061/(ASCE)PS.1949-1204.0000458

PREDICTING CRATER FORMATION FROM FAILURE OF PRESSURISED WATER MAINS THROUGH ANALOGY WITH BURIED EXPLOSIVE EVENTS

Andrew D. Barr, Ph.D [1]; Sam E. Rigby, Ph.D [2]; Richard Collins, Ph.D [3]; Vanessa Speight, Ph.D [4] and Thomas Christen [5]

ABSTRACT

Brittle failure of a buried pressurised water pipe can result in rapid crater formation and throw debris over large distances, as well as longer-term flooding and scour effects. Due to the potential for injury and property damage in a failure event, it is desirable to develop policies to enforce safe stand-off distances around high-risk pipes. Little published data is available on the formation of craters during the initial pressure release from a pipe burst, but an analogy can be made with buried explosives events, for which a large body of data exists. This paper uses finite-element modelling of buried pipe failures to assess the parameters affecting crater diameter, where pipe diameter, pressure, air content and burial depth are shown to be significant. An explosive cratering tool is modified for use with water pipes by converting the energy release from a failing pipe to an equivalent mass of explosive. The modified tool reliably replicates the crater size from the modelling results, and accurately predicts the modelled crater size in new failure scenarios ($r^2 = 0.95$), indicating the potential of the tool for use in developing policy around safe stand-off distances.

[1]Research Associate, Blast and Impact Dynamics, Dept. of Civil & Structural Engineering, The University of Sheffield, S1 3JD, UK. E-mail: a.barr@sheffield.ac.uk

[2]Lecturer, Blast and Impact Dynamics, Dept. of Civil & Structural Engineering, The University of Sheffield, S1 3JD, UK. E-mail: sam.rigby@sheffield.ac.uk

[3]Lecturer, Water Research Group, Dept. of Civil & Structural Engineering, The University of Sheffield, S1 3JD, UK. E-mail: r.p.collins@sheffield.ac.uk

[4]Senior Research Fellow, Water Research Group, Dept. of Civil & Structural Engineering, The University of Sheffield, S1 3JD, UK. E-mail: v.speight@sheffield.ac.uk

[5]Strategic Planner, Trunk Mains Team – Strategic Customer Service Planning, Scottish Water, 55 Buckstone Terrace, Fairmilehead, Edinburgh, EH10 6XH, UK. E-mail: thomas.christen@scottishwater.co.uk

Keywords: failure; cast iron; burial depth; crater; buried explosives; finite element modelling; safe stand-off distance

INTRODUCTION

The failure of large-diameter water mains can result in significant damage to nearby property and infrastructure. As well as the flooding risk associated with smaller pipes, large cast iron or pre-stressed concrete pipes can fail in a brittle manner and with little warning, releasing large volumes of pressurised water over a short time period. This sudden release of pressure can result in the rapid formation of craters and throw soil, rocks and ground cover debris over large distances, endangering public safety and adjacent properties (BBC News, 2017).

Besides regular inspection and maintenance of the network, the potential for damage can be mitigated by enforcing a stand-off distance between large-diameter pipes and the surrounding buildings, with further design requirements applied to any structures within this boundary. For example, the Washington Suburban Sanitary Commission used ten case studies of large-diameter breaks (mostly pre-stressed concrete, 900 mm to 2400 mm diameter) to recommend a 24 m (80 ft) stand-off distance based on recorded crater diameters and debris throw (WSSC, 2012).

Large-diameter pre-stressed concrete is not common in the UK water distribution network, which is instead dominated by cast and ductile iron pipes, the majority of which are below 1000 mm diameter. Failure of these pipes is likely to be less catastrophic than observed in the WSSC study, but this is balanced by the increased likelihood of failures in smaller-diameter pipes (Rajani et al., 1996) and in pipes constructed from cast iron (Rajeev et al., 2014).

The failure mechanism of cast iron pipes is dependent on diameter: pipes smaller than 380 mm (15 inches) tend to fail by circumferential cracking and pipes larger than 500 mm (20 inches) tend to fail with longitudinal cracks, while intermediate sizes may fail by spiral fracture (Makar et al., 2001). All diameters of cast and ductile iron pipe are susceptible to corrosion, which can lead to a sudden blow-out failure when combined with a pressure transient of sufficient magnitude (Jung et al., 2007). Even routine pump and valve operations can result in large transients with the potential to damage pipework: Rathnayaka et al. (2016) observed surges of up to 600 kPa (6 bar) while monitoring a distribution network under normal conditions. The risk of failure is magnified by the potential presence of volumes of air and other gases in the water pipes, which can occur due to either entrainment in pump systems or dissolved gases coming out of solution (Boulos et al., 2005).

An engineering assessment is required to develop policy on safe stand-off distances against these types of failures, and while little literature exists on the formation of craters due to water pipe failures, there is a large body of research on the craters produced by buried explosive events (e.g. Knox and Terhune (1965); Ambrosini and Luccioni (2006)). Like water pipe failures, buried explosions result in a sudden release of energy which can eject soil, and the size of the crater is related to the rate of energy release, the depth at which the release occurs and the properties of the surrounding soil and ground cover (Dillon, 1972).

Scaling laws have been developed for blast and impact processes to enable predictions of crater formation in events as varied as planetary impacts and nuclear explosions (Schmidt and Housen, 1987; Holsapple, 1993). These methods use dimensionless forms (Housen et al., 1983) and point-source approximations (Holsapple and Schmidt, 1987) to define a power law relationship between crater volume, the energy of the impact or explosion and the strength of the target material. The resulting scaling law reliably predicts experimental cratering results from the smallest to largest events (Holsapple and Schmidt, 1979).

This paper uses numerical modelling of bursts in buried water pipes to assess the effect of the initial pressure release on crater formation for a range of pipe diameters, burial depths and pressures. By equating the energy release in the burst pipe to an equivalent explosive mass, the modelling results are compared with predictions from scaling laws calibrated against a database of explosive cratering experiments (Holsapple, 2003a), and a cratering prediction tool is developed for pressurised water pipe bursts to help manage risk and inform the selection of safe stand-off distances.

MODELLING INITIAL CRATER FORMATION

There are several mechanisms which could contribute the energy available for cratering in a pipe burst event, namely: stress relief in the failing pipe wall; pressure relief of the water in the pipe; pressure relief of any trapped air in the pipe; and the continued water flow through the perforated pipe. The first three mechanisms occur almost immediately at the point of failure, while the scour from the continuing flow will occur over a longer period. As methods of estimating the effects of scour on long-term crater size have been reported elsewhere (van Daal et al., 2011; WSSC, 2012), this paper will focus on quantifying the initial cratering event, which is often completed before building occupants, pedestrians or road users have had time to react.

Calculations of the strain energy contained in the pipe wall, water and air in a pressurised pipe indicate that the dominant factor leading to a crater is the release of pressurised air from the pipe. For example, in a cast iron pipe with an internal diameter of 200 mm, wall thickness of 10 mm, pressure of 20 bar and 10% air by volume, the strain energy in the pipe wall (4 J/m) and water (25 J/m) are negligible compared to the air (180700 J/m). This also suggests that pipe material should have no effect on the formation of a crater other than the pressure at failure, and so the modelling considers how the pressure and volume of air and the pipe geometry affect crater formation, without directly considering the pipe material.

In buried explosive events a number of factors are known to affect crater size, including the explosive mass, depth of burial, and soil strength. Larger masses of explosive have a greater energy release and result in a larger crater. Increasing the depth of burial initially increases crater size, but very deep burial results in smaller craters (Chabai, 1965), eventually leading to a camouflet which does not break the ground surface. The greater the shear strength of the soil a pipe is buried in, the smaller the crater produced (Dillon, 1972). These parameters are analogous to those in a sudden pipe failure, if the explosive mass is instead equated to the energy in the pipe. Assuming that pipe material is neglected, parameters with the potential to affect the rate of energy release from the failed pipe are pipe diameter, pressure, air content, crack width and crack orientation.

Modelling setup

To assess the influence of these factors, a numerical study was performed using LS-DYNA, a commercial explicit finite element analysis software, using the multi-material arbitrary Lagrangian-Eulerian (MM-ALE) solver. The pipes were modelled in 2D plane strain (i.e. assuming an infinite length of pipe) to reduce computation time, as a 3D model with sufficient pipe length would be impractically large. As this simplification means that the air in the pipe on either side of the burst is not directly modelled, a length parameter is introduced later in the paper to take this into account.

The computational domain size (3 m by 3 m) and finite element mesh size (0.01 m) were informed by an initial mesh sensitivity study which is omitted here for brevity. The domain was divided vertically into 1.5 m of air and 1.5 m of soil, as shown in Fig. 1, and a pipe of diameter D was positioned at a burial depth of d_b. As the behaviour of the pipe was not being considered, rigid pipe 'walls' were created by adding displacement restraints to the elements on the circumference of the water part. Pipe damage was represented by removing this restraint over a segment θ degrees wide, allowing water and air to pass through. This crack was either positioned at the crown of the pipe (Fig. 1a) or at 45 degrees to the vertical (Fig. 1b). Where the crack was at the crown of the pipe, a vertical symmetry plane was introduced through the centre of the pipe to reduce computation time.

Water in the pipe was modelled using the equation of state described by Shin et al. (1998), and was pressurised to a pressure P. The air was modelled as an ideal gas with density $\rho = 1.225\ \mathrm{kg/m^3}$. Above ground level the air was initialised at atmospheric pressure (101 kPa), air in the pipe was pressurised to match the water with pressure P. The soil around the pipe was modelled using the equation of state and shear data for a well-characterised sand from high pressure quasi-static experiments (Barr et al., 2018, 2019). Strain rate effects were not explicitly modelled, as strain rate was shown to have no influence on the stiffness of this sand between quasi-static and high strain rates, and research on shear in soils at high strain strain rates is still ongoing (Barr et al., 2016). Data for wet sand (7% moisture content) was used, as this increases compressibility and decreases the shear strength of the soil, providing a more conservative estimate of crater size.

Sensitivity study

The parameter values used in the sensitivity study are shown in Table 1. As this 'explosive' failure mode is a high-energy event, relatively large values of pipe pressure and air volume have been selected. However, these encompass the typical pipe sizes and burial conditions (Twort et al., 2000), maximum potential pressures (Rathnayaka et al., 2016) and air volumes (Pozos et al., 2010) observed by other researchers. The crater size produced using each combination is shown in Table 2. Full expansion of the compressed air occurred over approximately a tenth of a second: while this is slow compared to the detonation of buried explosives, it highlights the risk to life and property represented by these events.

Pipe diameter had a large effect on crater size (Fig 2), as this directly affected the volume of air in the pipe at a given air content. The 300 mm and 500 mm pipe models both predicted a significant crater, while the 100 mm model predicted a camouflet, where the air bubble does not break the surface and instead forms an underground void. It is worth noting that because the soil is modelled as a continuum it tends to stretch into thin shells around the expanding air bubble. These soil shells have been observed in buried explosive experiments on wet soils, although tensile failure of the soil, and venting of the detonation products, would be expected to occur as expansion continued (Clarke et al., 2015). As the soil remains in contact with the detonation products for longer in the current modelling strategy, the results represent a conservative upper bound.

Crack orientation affected the shape of the expanding air bubble (Fig. 3) but did not significantly change crater diameter. The 45° cracks resulted in a crater which was offset from the centreline of the pipe: by 200 mm in the 300 mm pipe and by 350 mm in the 500 mm pipe, or approximately 15% of the crater diameter in each case. As crater diameter was unaffected by crack orientation, all subsequent models were performed using a crack at the crown of the pipe.

As failure of the 100 mm diameter pipe resulted in a camouflet at 500mm depth, deeper burial depths were only tested for the 300 mm and 500 mm diameter pipes. For 300 mm pipes an increase in burial depth decreased the crater size until a camouflet was formed, while for 500 mm pipes an increase in burial depth continued to increase the crater size. This is similar to studies on explosive cratering, where larger explosive devices have a larger 'optimum' burial depth (in terms of maximum crater size) (Chabai, 1965).

Models which varied the width of the crack in the pipe produced almost identical craters in each case, indicating that the geometry of the crack does not significantly affect crater size. As would be expected, a reduction in either pipe pressure or air volume led to a decrease in crater diameter.

In summary, the width and orientation of the crack in the pipe wall did not affect crater size, while pipe diameter, depth of burial, pipe pressure, and the percentage of pipe filled with air all had a significant effect. The pipe diameter, pipe pressure and percentage of air parameters all modify the energy stored in the compressed air in the pipe, and so it should be possible to equate this energy to an explosive mass for use in an existing explosive cratering tool, which also considers burial depth.

PREDICTING INITIAL CRATER FORMATION

Craters formed by buried explosives

The *Impacts and Explosion Effects* tool (Holsapple, 2003a) uses scaling laws (Holsapple and Schmidt, 1979; Schmidt and Housen, 1987) and an analysis of over 900 craters to predict crater formation based on the energy of a blast or impact event. The tool uses an equation formed of four dimensionless groups:

$$\pi_v = FK_1 \left[\pi_2 \left(\frac{\rho}{\delta} \right)^{\frac{6v-2-\mu}{3\mu}} + K_2 \left(\pi_3 \left(\frac{\rho}{\delta} \right)^{\frac{6v-2}{3\mu}} \right)^{\frac{2+\mu}{2}} \right]^{\frac{-3\mu}{2+\mu}} \tag{1}$$

where π_v is the normalised crater volume,

$$\pi_v = \frac{\rho V}{W} \tag{2}$$

π_2 controls the effects of gravity,

$$\pi_2 = \frac{g}{Q} \left(\frac{W}{\delta} \right)^{\frac{1}{3}} \tag{3}$$

and π_3 controls the effects of soil strength,

$$\pi_3 = \frac{Y}{\rho Q} \tag{4}$$

Soil density and strength are defined using ρ and Y, while K_1, K_2, μ and ν are additional soil coefficients/ exponents which can be calculated using fits to experimental data. The explosive density, specific energy, mass, radius and burial depth are given by δ, Q, W, a and d, and g is the acceleration due to gravity. Units for these parameters are provided in the *Notation* section. F is a function of explosive charge radius, a, and burial depth, d, which controls the effect of burial depth on crater size, and is defined as

$$F = 1.92 \left(\frac{d}{a} \right)^{\frac{3\mu}{2+\mu}} \tag{5}$$

Holsapple (2003b) provides calculated soil coefficients and exponents for several soil and rock types. The most appropriate values for this work are those for 'wet soil', where $K_1 = 0.051$, $K_2 = 1$, $\mu = 0.55$, $\nu = 0.33$, $Y = 0.35$ MPa, and $\rho = 2100$ kg/m^3. These values were calibrated using experimental data for cratering (e.g. Schmidt and Housen (1987)), and cover all cases from sub-gram centrifuge tests up to large nuclear events. It should be noted that K_1 and Y are calculated as the product $K_1 Y$, and K_1 is then assigned a value of unity. As a result the 'strength' parameter Y does not directly represent the strength of the soil.

To use the tool, all known values for the soil, explosive, burial depth and gravity are input into the formula. This provides a value of π_v, which is multiplied by the explosive charge mass to find the mass of the crater, then divided by the soil density to find the volume of the crater. Coefficients on crater shape are defined to convert this volume into a crater radius (using K_r) and depth (using K_d), again based on the database of experimental data. For example, the crater radius is calculated as

$$r = K_r V^{\frac{1}{3}} \tag{6}$$

where $K_r = 1.1$ and $K_d = 0.6$ for 'wet soil'.

Craters formed by failing water pipes

As the *Impacts and Explosion Effects* tool is designed to estimate the craters produced by buried explosions, several modifications are required to make it suitable for use with failing water pipes:

- conversion of the energy in the compressed air into an equivalent explosive mass;
- representation of the plane strain modelling results as a point explosive event; and
- modification of the function controlling burial depth effects (Eq. 5) to reduce crater diameter below the optimum burial depth.

To convert the compressed gas in the pipe into an equivalent explosive mass, the energy released by the gas as it expands, E, is divided by the specific energy of TNT, $Q = 4.19$ MJ/kg. Assuming adiabatic gas expansion, the equivalent explosive mass, W_{eq} is

$$W_{\mathrm{eq}} = \frac{E}{Q} = \frac{P_2V_2 - P_1V_1}{Q(1-\gamma)} \tag{7}$$

where P_1 and V_1 are the compressed pressure and volume, P_2 and V_2 are the pressure and volume after expansion to atmospheric pressure, and γ is the ratio of specific heats, equal to 1.4 for air. Eq. 1 also requires the radius, a, of this spherical explosive, which can be calculated from W using the density of TNT, $\delta = 1640$ kg/m^3.

To convert the plane strain models to a point explosive event, a factor, L, was applied to the calculated cross-sectional area of gas in the pipe, acting as the 'length' of air used in the calculation of V_1 in Eq. 7. This factor was calculated as $L = 20$ m (i.e. 10 m each side of the burst) by comparing the modelled and calculated results for pipe geometries with low d/a ratios, as it was known that the burial depth factor, F, would also need to be modified for higher d/a values.

As written, the value of F will increase indefinitely as the burial depth increases, though experiments show that after an 'optimal' burial depth the crater size decreases rapidly (Chabai, 1965). To incorporate this, the modified factor F_{mod} reaches a peak at the optimum value, $\left(\frac{d}{a}\right)_{\mathrm{opt}}$, then decreases, approaching zero at $d/a = 20$. Using the modelled examples, optimum values were selected as $\left(\frac{d}{a}\right)_{\mathrm{opt}} = 8$ for $D \leq 400$ mm, and $\left(\frac{d}{a}\right)_{\mathrm{opt}} = 16$ for $D > 400$ mm. All events with a d/a greater than 20 are assumed to be camouflets:

$$F_{\mathrm{mod}} = \begin{cases} 1.92\left(\frac{d}{a}\right)^{\frac{3\mu}{2+\mu}}, & \text{if } 0 \leq \frac{d}{a} \leq \left(\frac{d}{a}\right)_{\mathrm{opt}} \\ \frac{1.92\left(\frac{d}{a}-20\right)\left(\frac{d}{a}\right)^{\frac{3\mu}{2+\mu}}}{\left(\frac{d}{a}\right)_{\mathrm{opt}}-20}, & \text{if } \left(\frac{d}{a}\right)_{\mathrm{opt}} < \frac{d}{a} \leq 20 \\ 0 \text{ (camouflet)}, & \text{if } \frac{d}{a} > 20 \end{cases} \tag{8}$$

A worked example of using the modified cratering prediction tool is provided in Appendix I.

Validation of crater prediction tool

A comparison of the crater diameters predicted through modelling and the modified cratering tool is shown in Table 2 and by the filled circles in Fig. 4. These results show that the modified cratering tool can predict the crater diameter for the modelled calibration cases to within 200 mm, with an r^2 value of 0.95. To ensure that this accuracy can be maintained with other combinations of input parameters, three additional validation models were run in LS-DYNA with pipe diameters of 200mm and 400mm, as shown in Table 3. These events were also well predicted by the cratering tool, and are marked using the unfilled circles in Fig. 4.

While this paper is primarily concerned with medium-diameter pipes, two additional models were run to assess the cratering tool's ability to calculate crater sizes for larger 1200mm diameter pipes. Two additional LS-DYNA models were run for 1200mm pipes at burial depths of 500mm and 1000mm, as shown in Table 3. As indicated by the crosses on Fig. 4, the cratering tool slightly under-predicts the initial crater diameter on these large pipes. However, on a pipe of this size any small error is unlikely to have a significant effect on the final crater size, as the flow rates in these pipes are likely to lead to significant scour effects over a short period of time.

The modified cratering tool can reliably predict the plane strain modelling results over a range of input parameters, but a comparison with experimental data would be required to enable accurate prediction of a burst in a live system. This would be limited to recalculating the value of L, the length of compressed air in the pipe contributing to the burst, to ensure the correct initial energy is calculated: all other parameters would remain unchanged.

CONCLUSION

A sensitivity study was performed on the parameters affecting the initial crater produced by the sudden brittle failure of medium-diameter buried water pipes. In LS-DYNA finite-element models, high energy failures resulted in craters as expected, while some low-intensity or deeply-buried failures resulted in an underground void which did not immediately form a crater (a camouflet). Crater formation occurred in less than a tenth of a second, highlighting the importance of developing safe stand-off distance policy where failure could result in loss of life or serious property damage. The width and orientation of the crack at failure did not significantly affect crater size, which was controlled primarily by pipe diameter, depth of burial, pipe pressure at failure and the air content of the pipe. These parameters describe a rapid release of energy at a certain depth in the soil, similar to the detonation of a buried explosive, and so enabled comparison with the existing explosive cratering literature.

A cratering prediction tool, based on a large database of explosive experiments, was modified to suit the case of water pipe failures. The energy released by air in the failing pipe was converted to an equivalent explosive mass assuming adiabatic expansion, and a factor controlling the effect of burial depth was modified to more accurately represent the case of buried pipes. The modified tool reliably replicated the crater size from the LS-DYNA modelling results, and could also accurately predict the modelled crater size in new failure scenarios for medium-diameter pipes ($r^2 = 0.95$). While further calibration against experimental bursts would be required to accurately predict physical bursts, this result indicates the potential of the tool for use in developing policy for safe stand-off distances, and particularly for understanding the immediate risks surrounding sudden water pipe failures before related scour and flooding effects can occur.

APPENDIX I. WORKED EXAMPLE

As an example of using the modified cratering prediction tool, consider the case of a 500 mm diameter pipe buried at a depth of 750 mm in the wet soil described above. At the point of failure the pipe is pressurised to 30 bar with an air content of 15%, and a failure occurs at the crown.

Equivalent explosive mass

The volume of compressed air in the pipe is

$$V_1 = \frac{A_v}{100} \cdot L\pi \left(\frac{D}{2}\right)^2 = \frac{15}{100} \cdot 20\pi \left(\frac{0.5}{2}\right)^2 = 0.589 \text{ m}^3, \tag{9}$$

and the volume at atmospheric pressure ($P_2 = 101$kPa) is

$$V_2 = V_1 \left(\frac{P_1}{P_2}\right)^{\frac{1}{\gamma}} = 0.589 \left(\frac{3 \times 10^6}{101 \times 10^3}\right)^{\frac{1}{1.4}} = 6.640 \text{ m}^3. \tag{10}$$

Using Eq. 7, explosive mass equivalent to the energy in the adiabatic expansion of the air is then

$$W_{\text{eq}} = \frac{P_2V_2 - P_1V_1}{Q(1-\gamma)} = \frac{(101 \times 10^3 \cdot 6.640) - (3 \times 10^6 \cdot 0.589)}{(4.19 \times 10^6)(1 - 1.4)} = 0.658 \text{ kg}, \tag{11}$$

and the radius of this explosive can be calculated as

$$a = \left(\frac{3}{4\pi}\frac{W_{\text{eq}}}{\delta}\right)^{\frac{1}{3}} = \left(\frac{3}{4\pi}\frac{0.658}{1640}\right)^{\frac{1}{3}} = 0.046 \text{ m}. \tag{12}$$

Effect of burial depth

The ratio d/a for this explosive is $0.75/0.046 = 16.3$, near the optimum value of $\left(\frac{d}{a}\right)_{\text{opt}} = 16$ for this pipe diameter. The modified burial depth factor F_{mod} can be calculated using Eq. 8 as:

$$F_{\text{mod}} = \frac{1.92\left(\frac{d}{a} - 20\right)\left(\frac{d}{a}\right)^{\frac{3\mu}{2+\mu}}}{\left(\frac{d}{a}\right)_{\text{opt}} - 20} = \frac{1.92(16.3-20)(16.3)^{\frac{3 \cdot 0.55}{2+0.55}}}{16-20} = 10.8. \tag{13}$$

Normalised groups

The normalised groups in Eqs. 3 and 4 can now be solved and substituted into Eq. 1 using the soil parameters from Holsapple (2003b), where $K_1 = 0.051$, $K_2 = 1$, $\mu = 0.55$, $\nu = 0.33$, $Y = 0.35$ MPa, and $\rho = 2100$ kg/m^3:

$$\pi_2 = \frac{g}{Q}\left(\frac{W_{\mathrm{eq}}}{\delta}\right)^{\frac{1}{3}} = \frac{9.81}{4.19 \times 10^6}\left(\frac{0.658}{1640}\right)^{\frac{1}{3}} = 1.727 \times 10^{-7} \tag{14}$$

$$\pi_3 = \frac{Y}{\rho Q} = \frac{3.5 \times 10^5}{2100 \cdot 4.19 \times 10^6} = 3.978 \times 10^{-5} \tag{15}$$

$$\begin{aligned}
\pi_v &= F_{\mathrm{mod}} K_1 \left[\pi_2 \left(\frac{\rho}{\delta}\right)^{\frac{6v-2-\mu}{3\mu}} + K_2 \left(\pi_3 \left(\frac{\rho}{\delta}\right)^{\frac{6v-2}{3\mu}}\right)^{\frac{2+\mu}{2}}\right]^{\frac{-3\mu}{2+\mu}} \\
&= 10.8 \cdot 0.051 \left[1.727 \times 10^{-7} \left(\frac{2100}{1640}\right)^{\frac{6\cdot 0.33-2-0.55}{3\cdot 0.55}}\right. \\
&\qquad \left. +1 \left(3.978 \times 10^{-5} \left(\frac{2100}{1640}\right)^{\frac{6\cdot 0.33-2}{3\cdot 0.55}}\right)^{\frac{2+0.55}{2}}\right]^{\frac{-3\cdot 0.55}{2+0.55}} \\
&= 2263
\end{aligned} \tag{16}$$

Rearranging Eq. 2 then provides the volume of the crater,

$$V = \frac{\pi_v W_{\mathrm{eq}}}{\rho} = \frac{2263 \cdot 0.658}{2100} = 0.709 \text{ m}^3 \tag{17}$$

which can be expressed as a radius using the shape factor K_r,

$$r = K_r V^{\frac{1}{3}} = 1.1 \cdot 0.709^{\frac{1}{3}} = 0.98 \text{ m}. \tag{18}$$

That is, this example will result in a crater with a diameter of 1.96 m.

APPENDIX II. DATA AVAILABILITY STATEMENT

Keyword files and MATLAB scripts used for numerical modelling in LS-DYNA are available from the corresponding author by request.

APPENDIX III. ACKNOWLEDGEMENTS

This work forms part of the Scottish Water-funded project "Refinement of safe stand-off distances associated with pressurised water mains". The authors would particularly like to thank Ross O'Rourke of RPS Water for his contributions to this paper.

APPENDIX IV. NOTATION

The following symbols are used in this paper:

D = pipe diameter (m);
E = energy released by expanding air (J);
F = burial depth factor;
F_{mod} = modified burial depth factor;
K_1 = soil coefficient;
K_2 = soil coefficient;
K_d = crater depth coefficient;
K_r = crater radius coefficient;
L = length of air volume (m);
P = pressure (Pa);
P_1 = initial air pressure in pipe (Pa);
P_2 = expanded air pressure (Pa);
Q = explosive specific energy (J/kg);
V = crater volume (m^3);
V_1 = initial volume of air in pipe (m^3);
V_2 = volume of expanded air (m^3);
V_a = volume of pipe filled with air (%);
W = explosive charge mass (kg);
W_{eq} = equivalent explosive charge mass (kg);
Y = soil shear strength (Pa);
a = explosive charge radius (m);
d = explosive burial depth, to centre (m);
d_b = pipe burial depth, to crown (m);
g = acceleration due to gravity (m/s^2);
r = crater radius (m);
γ = adiabatic gas constant;
δ = density of explosive (kg/m^3);
θ = crack width (degrees);
θ_r = crack orientation (degrees);
μ = soil exponent;
ν = soil exponent;
π_2 = normalised gravity term;
π_3 = normalised strength term;
π_v = normalised crater volume;
ρ = soil density (kg/m^3);

REFERENCES

Ambrosini, R. D. and Luccioni, B. M. (2006). "Craters produced by explosions on the soil surface." *Journal of Applied Mechanics*, 73(6), 890–900.

Barr, A. D., Clarke, S. D., and Petkovski, M. (2019). "High-pressure compressibility and shear strength data for soils." *Canadian Geotechnical Journal*, 56(7).

Barr, A. D., Clarke, S. D., Rigby, S. E., Tyas, A., and Warren, J. A. (2016). "Design of a split Hopkinson pressure bar with partial lateral confinement." *Measurement Science and Technology*, 27(12), 125903.

Barr, A. D., Clarke, S. D., Tyas, A., and Warren, J. A. (2018). "Effect of moisture content on high strain rate compressibility and particle breakage in loose sand." *Experimental Mechanics*, 58, 1331–1334.

BBC News (2017). "Dramatic Ukraine water pipe explosion captured on CCTV, <https://www.bbc.co.uk/news/av/world-europe-40101394>.

Boulos, P. F., Karney, B. W., Wood, D. J., and Lingireddy, S. (2005). "Hydraulic transient guidelines for protecting water distribution systems." *Journal-American Water Works Association*, 97(5), 111–124.

Chabai, A. J. (1965). "On scaling dimensions of craters produced by buried explosives." *Journal of Geophysical Research*, 70(20), 5075–5098.

Clarke, S., Rigby, S., Fay, S., Tyas, A., Reay, J., Warren, J., Gant, M., Livesey, R., and Elgy, I. (2015). "Bubble-type vs shock-type loading from buried explosives." *Proceedings of the 16th International Symposium on Interaction of the Effects of Munitions with Structures (ISIEMS16)*, Destin, FL, USA.

Dillon, L. A. (1972). "The influence of soil and rock properties on the dimensions of explosion-produced craters." *Report No. AFWL-TR-71-144*, Air Force Weapons Laboratory, Kirtland AFB.

Holsapple, K. (1993). "The scaling of impact processes in planetary sciences." *Annual review of earth and planetary sciences*, 21(1), 333–373.

Holsapple, K. and Schmidt, R. (1979). "A material-strength model for apparent crater volume." *Lunar and Planetary Science Conference Proceedings*, Vol. 10, 2757–2777.

Holsapple, K. and Schmidt, R. (1987). "Point source solutions and coupling parameters in cratering mechanics." *Journal of Geophysical Research: Solid Earth*, 92(B7), 6350–6376.

Holsapple, K. A. (2003a). "Impact and explosion effects, <http://keith.aa.washington.edu/craterdata/scaling/index.htm>.

Holsapple, K. A. (2003b). *Theory and equations for Craters from Impacts and Explosions.* St. Louis, MO: Washington University.

Housen, K., Schmidt, R., and Holsapple, K. (1983). "Crater ejecta scaling laws: Fundamental forms based on dimensional analysis." *Journal of Geophysical Research: Solid Earth*, 88(B3), 2485–2499.

Jung, B. S., Karney, B. W., Boulos, P. F., and Wood, D. J. (2007). "The need for comprehensive transient analysis of distribution systems." *American Water Works Association*, 99(1).

Knox, J. B. and Terhune, R. W. (1965). "Calculation of explosion-produced craters - High-explosive sources." *Journal of Geophysical Research*, 70(10).

Makar, J. M., Desnoyers, R., and McDonald, S. E. (2001). "Failure modes and mechanisms in gray cast iron pipes." *Underground Infrastructure Research*, 1–11.

Pozos, O., Sanchez, A., Rodal, E. A., and Fairuzov, Y. V. (2010). "Effects of water–air mixtures on hydraulic transients." *Canadian Journal of Civil Engineering*, 37(9), 1189–1200.

Rajani, B., Zhan, C., and Kuraoka, S. (1996). "Pipe-soil interaction analysis of jointed water mains." *Canadian Geotechnical Journal*, 33, 393–404.

Rajeev, P., Kodikara, J., Robert, D., Zeman, P., and Rajani, B. (2014). "Factors contributing to large diameter water pipe failure." *Water Asset Management International*, 10(3), 9–14.

Rathnayaka, S., Shannon, B., Rajeev, P., and Kodikara, J. (2016). "Monitoring of pressure transients in water supply networks." *Water Resources Management*, 30(2), 471–485.

Schmidt, R. M. and Housen, K. R. (1987). "Some recent advances in the scaling of impact and explosion cratering." *International Journal of Impact Engineering*, 5(1-4), 543–560.

Shin, Y. S., Lee, M., Lam, K. Y., and Yeo, K. S. (1998). "Modeling mitigation effects of watershield on shock waves." *Shock and Vibration*, 5(4), 225–234.

Twort, A. C., Ratnayaka, D. D., Brandt, M. J., et al. (2000). *Water supply*. Elsevier.

van Daal, K., Beuken, R., Vogelaar, A., and Diemel, R. (2011). "The impact of a pipe burst on the surrounding area integrating GIS and hydraulic modelling in a risk based approach." *Leading Edge Conference on Strategic Asset Management*, Mülheim an der Ruhr, Germany.

WSSC (2012). "WSSC pipeline design manual amendment - proposed 80-foot setback." *Report No. 301-206-WSSC*, Washington Suburban Sanitary Commission.

List of Tables

TABLE 1. Model pipe parameters used in sensitivity study.

Symbol	Parameter	Value range
D	Pipe diameter, mm	100, 300, 500
d_b	Depth of burial, mm	500, 750, 1000
P	Pipe pressure (water and air), bar	10, 20, 30
V_a	Percentage of pipe filled with air, %	20, 30, 40
θ	Width of crack, degrees	20, 50, 90
θ_r	Crack orientation, degrees	0, 45

TABLE 2. Model sensitivity study results.

Variable	D, mm	d_b, mm	P, bar	V_a, %	θ, °	θ_r, °	Modelled crater diameter, m	Cratering tool prediction, m
Pipe diameter ($\theta_r = 0°$)	100	500	30	40	20	0	0.3[a]	0.4[b]
	300	500	30	40	20	0	1.6	1.7
	500	500	30	40	20	0	2.3	2.3
Pipe diameter ($\theta_r = 45°$)	100	500	30	40	20	45	0.2[a]	0.4[b]
	300	500	30	40	20	45	1.6	1.7
	500	500	30	40	20	45	2.3	2.3
Burial depth (300 mm pipe)	300	500	30	40	20	0	1.6	1.7
	300	750	30	40	20	0	1.4	1.4
	300	1000	30	40	20	0	1.0[a]	0.9[b]
Burial depth (500 mm pipe)	500	500	30	40	20	0	2.3	2.3
	500	750	30	40	20	0	2.6	2.5
	500	1000	30	40	20	0	2.8	2.7
Effect of crack width	300	500	30	40	20	0	1.6	1.7
	300	500	30	40	50	0	1.6	1.7
	300	500	30	40	90	0	1.6	1.7
Pipe pressure	300	500	30	40	20	0	1.6	1.7
	300	500	20	40	20	0	1.1	1.3
	300	500	10	40	20	0	0.8	0.9
Air volume	300	500	30	40	20	0	1.6	1.7
	300	500	30	30	20	0	1.1	1.5
	300	500	30	20	20	0	1.0	1.3

[a] These models resulted in a camouflet of the indicated diameter. A camouflet is when an underground void is formed with little effect at the ground surface. In a camouflet flow from the damaged pipe may cause the initial damage to progress to form a crater.

[b] Cratering tool predicts a camouflet.

TABLE 3. Cratering tool validation results.

Variable	D, mm	d_b, mm	P, bar	V_a, %	θ, °	θ_r, °	Modelled crater diameter, m	Cratering tool prediction, m
Model validation	400	500	30	40	20	0	2.0	2.1
	400	500	30	20	20	0	1.6	1.8
	200	500	30	20	20	0	0.5	0.7
1200 mm pipes	1200	1000	20	30	20	0	4.0	3.5
	1200	500	20	30	20	0	3.4	3.1

List of Figures

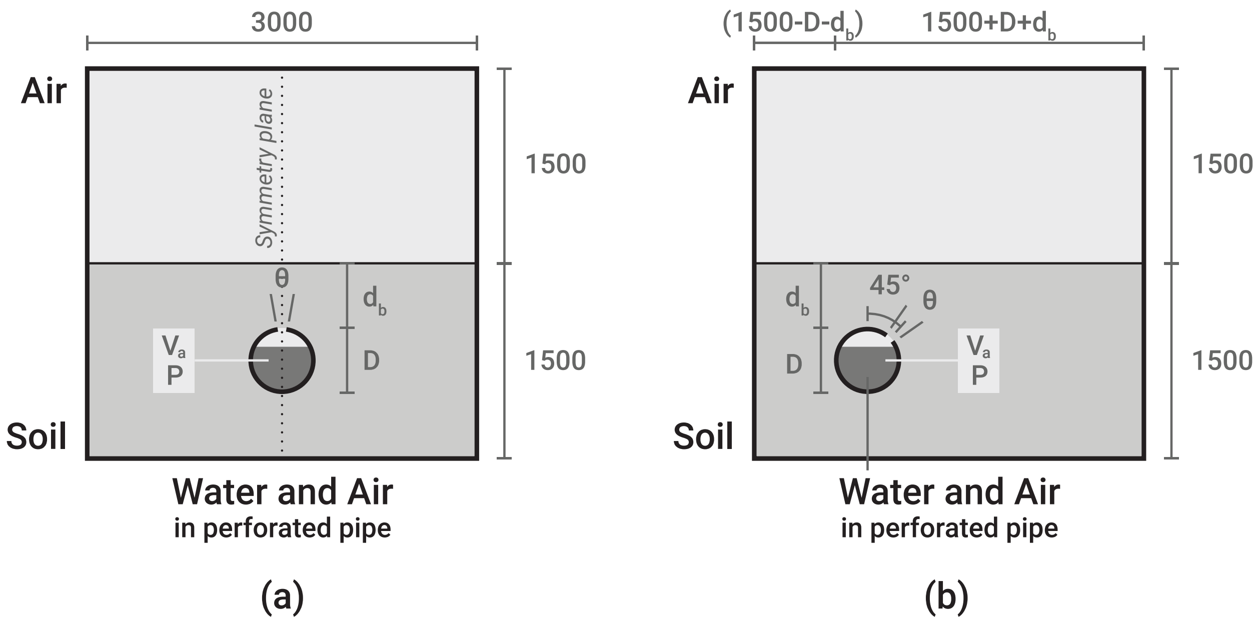

FIG. 1. Modelling domains and key variables for a) cracks at the crown of the pipe and b) cracks at 45 degrees to the vertical.

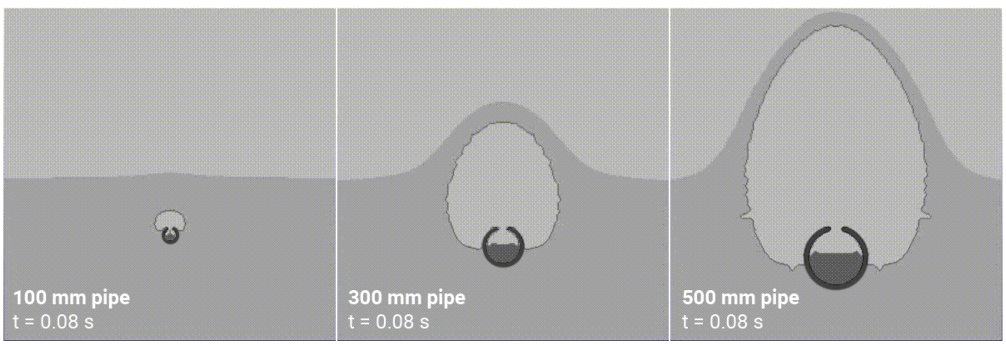

FIG. 2. Effect of pipe diameter on crater size.

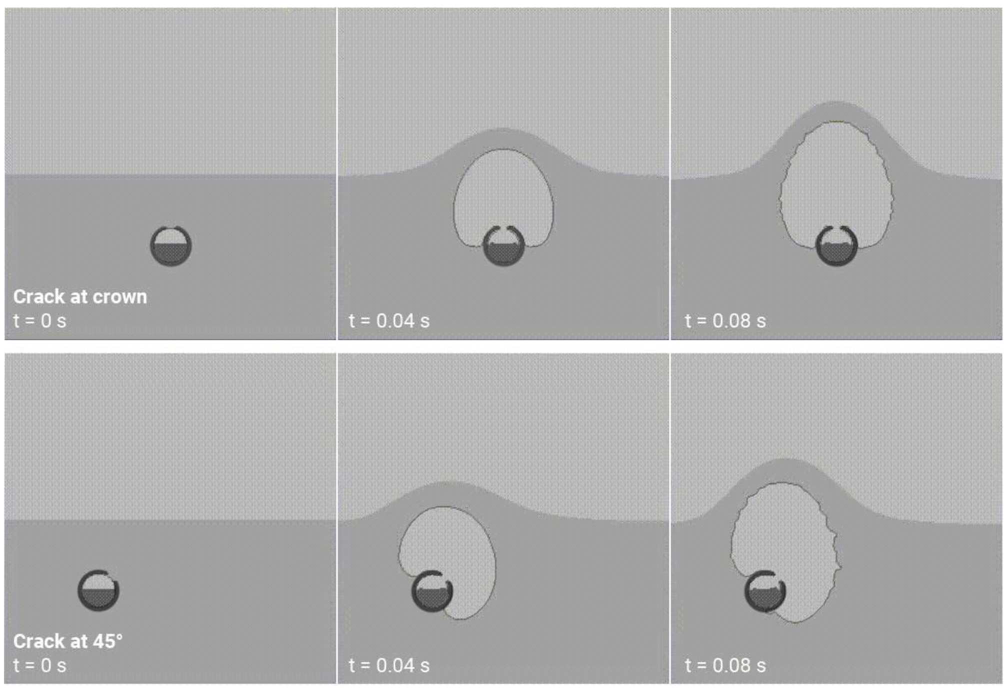

FIG. 3. Effect of crack orientation on crater size.

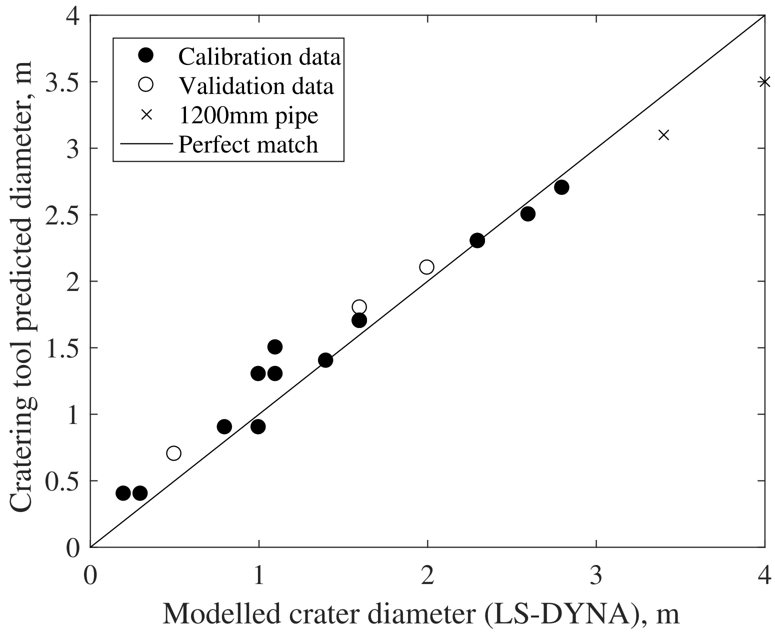

FIG. 4. Correlation of cratering tool predictions of crater diameter with LS-DYNA models.